Precision Lamb-shift measurement in the $n = 2$ state of $^6Li^{2+}$

M. Leventhal
Bell Laboratories, Murray Hill, New Jersey 07974
(Received 5 November 1974)

A microwave-optical-pulsing and trapping technique has been employed to observe Lamb-shift ($\mathcal{S} = 2S_{1/2} \rightarrow 2P_{1/2}$) transitions in $^6Li^{2+}$. Microwave transitions were induced in trapped metastable $Li^{2+}(2S_{1/2})$ ions produced beforehand by a pulsed electron beam incident upon a low-pressure lithium vapor. Resonances were observed in the soft x-ray decay light as an applied magnetic field was swept through the Zeeman transition frequency. Computer fitting of 76 line centers yields $\mathcal{S} = 62\,765 \pm 21$ MHz, in good agreement with theory.

I. INTRODUCTION

Precise Lamb-shift measurements in the first excited state of H, D, and $^4He^+$ have historically provided important fundamental tests of quantum electrodynamics (QED).[1] The results of these experiments are summarized in Table I along with the results of some less precise measurements in more highly ionized systems. We report here the results of an attempt to take the next logical step in this sequence, i.e., a precise $\mathcal{S}$ measurement in the $n=2$ state of $^6Li^{2+}$. (An abbreviated report of this work has been published elsewhere.[2]) A less accurate measurement by the nonresonant Stark-quenching technique is tabulated in Table I and agrees with the present result.[3] In addition, several other groups are actively pursuing precision measurement in this state[4] and in even more highly ionized systems.[5,6] The continuing interest in extending the measurements to Li^{2+} and beyond stems from the strong Z (nuclear charge) dependence of the conventional QED double expansion for $\mathcal{S}$[7] in α and $Z\alpha$:

$$\mathcal{S} = \sum_{i,j \geq 4} \alpha^i (Z\alpha)^j C_{ij}, \tag{1}$$

where α is the fine-structure constant and the C_{ij} are term coefficients, which are either independent or slowly varying functions of Z. The measurements provide progressively more rigorous tests of the higher-order terms in $Z\alpha$ and hence of our basic understanding of the virtual radiative processes involved. As can be seen from Table I, no significant disagreement between theory and experiment exists at this time.

From a calculational point of view the measurements must eventually yield an interesting result. The higher-order coefficients whose importance is being systematically exaggerated by this sequence of measurements are becoming increasingly difficult to calculate [terms of order $\alpha(Z\alpha)^6$ and $\alpha^2(Z\alpha)^4$ have been calculated to date]. Eventually uncertainties associated with uncalculated higher-order terms must produce a real discrepancy between experiment and the conventional theory. In this light Erickson[8] has recently made a major improvement in the theory by obtaining a closed-form expression for the $Z\alpha$ part of the expansion in Eq. (1). Measurements like the one reported here should provide a definitive test of this new theory and others valid in the high-Z domain.

II. METHOD

The technique employed in the current work is a unique derivative of schemes employed in earlier experiments[9,10] and, like them, takes advantage of the metastability of the $2S_{1/2}$ state against optical decay to the $1S_{1/2}$ ground state. The $Li^{2+}(2S_{1/2})$ state decays eventually by a two-photon process with $\tau_{2S} = 1.67 \times 10^{-4}$ sec.[11] On the other hand, the $2P_{1/2}$ state, which lies ~62.7 GHz below the $2S_{1/2}$ state in zero magnetic field, decays rapidly ($\tau_{2P} = 1.98 \times 10^{-11}$ sec)[12] in the electric-dipole approximation with the emission of a 135-Å Lyα quantum (see Fig. 8). An elaborate microwave-optical-pulsing and trapping scheme takes advantage of this gross difference in lifetimes to allow direct observation of the $2S_{1/2}$-to-$2P_{1/2}$ resonant transition. While in principle the experiments should be quite straightforward, the feebleness of the signal and the pernicious way in which lithium attacks all experimental components has made for a difficult task. The complex scheme represents our effort to maximize the signal-to-noise ratio during the short time (~10 h) available before the apparatus must be recycled. An important compensating feature has been the relative insensitivity of the normalized resonance data to Stark effects. Since electric fields of the order of tens of V/cm produce negligible shifts of the line center, it has been possible to work in what might be considered a "dirty" environment and yet obtain a result reasonably free of systematic errors.

TABLE I. Lamb shift S in GHz for the $n=2$ state of hydrogenic atoms. Theory vs experiment. Measurements in the $n=3$ and $n=4$ states have not been tabulated for the sake of brevity. Good agreement is also observed for these states.

Species	Theory	Experiment	References
H	1.057 91 ± 0.000 01	1.057 90 ± 0.000 06	Robiscoe; Triebwasser, Dayhoff, Lamb Ref. 1
		1.057 77 ± 0.000 06	
D	1.059 259 ± 0.000 028	1.059 28 ± 0.000 06	Cosens; Triebwasser, Dayhoff, Lamb Ref. 1
		1.059 00 ± 0.000 06	
He^+	14.044 78 ± 0.000 68	14.0454 ± 0.0012	Narasimham, Strombotne; Lipworth, Novick Ref. 1
		14.0402 ± 0.0018	
Li^{2+}	62.762 ± 0.009	63.0310 ± 0.327	Fan, Garcia-Munoz, Sellin Ref. 3
C^{5+}	783.68 ± 0.25	780.1 ± 8.0	Kugel, Leventhal, Murnick Ref. 32
O^{7+}	2205.17 ± 1.56	2202.7 ± 11.0	Leventhal, Murnick, Kugel Ref. 35
		2215.6 ± 7.5	Lawrence, Fan, Bashkin Ref. 36

$Li^{2+}(2S_{1/2})$ metastables are made inside a vacuum chamber by the simultaneous double ionization and excitation of atomic lithium vapor upon electron bombardment (see Fig. 1). The Li vapor is produced by a molybdenum oven containing molten Li and directed to the interaction region (IR) by a crinkle-foil nozzle. The IR is situated at the center of a 15-in. Varian electromagnet which serves both to collimate the electron beam and to enable us to scan resonances between the Zeeman sublevels. The resonance observed in this experiment, βe, is between the $2S_{1/2}(m_J=-\frac{1}{2})$ and $2P_{1/2}(m_J=+\frac{1}{2})$ sublevels, which occur at a field $H_0 \approx 14.4$ kG for our driving frequency $\nu_0 \approx 35.8$ GHz (see Sec. III). Light coming from the interaction region is collected with the aid of a light pipe and directed through a thin Be film to a windowless photomultiplier sensitive to 135-Å radiation. The Be film serves as a narrow bandpass filter from about 100 to 300 Å and also protects the photomultiplier from Li attack. In addition, a small amount of krypton gas is made to flow continuously down the light pipe in order to extend the useful lifetime of the light collection system.

The data acquisition sequence outlined in Fig. 2 was designed to maximize the signal strength relative to an overwhelming background detected when the e-gun is on and also to provide a reliable normalization scheme to deal with time variations and effects associated with scanning the magnetic field many kilogauss across a resonance. The linewidth is determined predominantly by the $2P$-state lifetime and is about 4 kG FWHM (full width at half-maximum), corresponding to about 10 GHz. An e-gun and ion trap are pulsed on simultaneously by driving the cathode 650 V negative with respect to a grounded field-free drift region and applying +18 V to two reflector electrodes. Ion motion in the transverse direction is contained by the magnetic field. After allowing 6 μsec for the trap to fill with metastables the e-gun is turned off. This is followed by a 1-μsec delay which allows most of the background light to decay away. The micro-

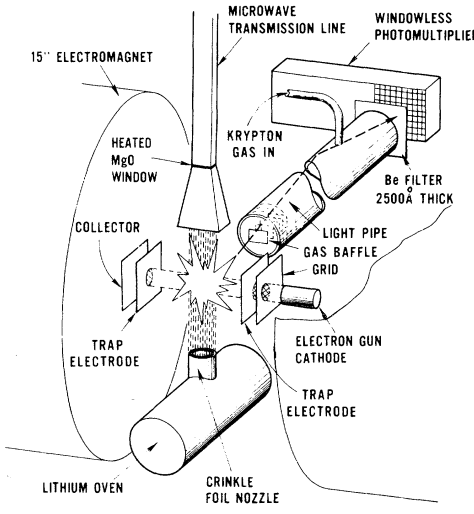

FIG. 1. Schematic diagram of the apparatus. The vacuum envelope is not shown.

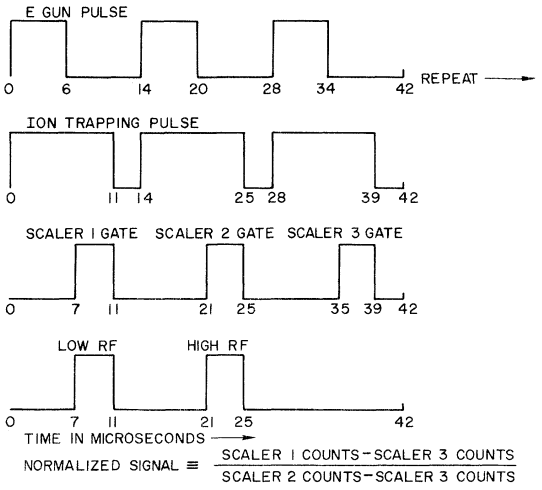

FIG. 2. Data acquisition sequence.

waves are then gated on and the scaler opened. Additional microwave-induced counts are then recorded as $2S_{1/2}$ atoms are driven to the $2P_{1/2}$ state, from which they rapidly decay. Data are acquired in this fashion at 14 fixed magnetic field points for three different microwave power levels: low, high, and off. At the high-power level, which is adequate to saturate the transition and broaden the resonance considerably, a 35% enhancement of the counting rate at the resonance center is typically observed. By defining the signal to be equal to

$$\frac{\text{(low-power counts)} - \text{(background counts)}}{\text{(high-power counts)} - \text{(background counts)}}$$

a normalized signal independent of a large class of possible asymmetries is obtained. In fact, the only asymmetries which remain uncancelled are those that affect the three unresolved hyperfine components ($I = 1$) differently.[10]

III. ENERGY LEVELS AND MATRIX ELEMENTS

In the absence of a magnetic field the $n = 2$ term consists basically of a triplet of levels[13] ($2S_{1/2}$, $2P_{1/2}$, and $2P_{3/2}$) which can be characterized by three quantities: the Lamb shift $\mathcal{S}$, the fine-structure splitting ΔE, and the hyperfine splitting of the $2S_{1/2}$ level ΔW. In Fig. 4 this term is indicated showing the $2S_{1/2}$ and $2P_{3/2}$ levels raised above the $2P_{1/2}$ level by $\mathcal{S}$ and ΔE, respectively. The additional hyperfine splitting of these levels is in general too small to be seen on the scale of Fig. 4. The values of $\mathcal{S}$, ΔE, and ΔW employed are shown in Table II along with other parameters used in determining theoretical energy levels. Since neither ΔE nor ΔW has been measured experimentally, theoretical values have been used. Fortunately, the experimental determination of $\mathcal{S}$ is insensitive to these parameters and no additional uncertainty is introduced.

For reasons of experimental convenience the measurement has been performed in a large magnetic field. Hence a primary task is to determine accurate values of the Zeeman sublevels and di-

TABLE II. Physical constants used in the Hamiltonian and in the data analysis.

Symbol	Value	Reference
$\mathcal{S}$	62 749 MHz	16
	62 762 MHz	17
ΔE	889 137 MHz	16
ΔW	1060.5 MHz	18
g_S	2.002 319 1	19
g_L	0.999 908 8	20
g_I	−0.000 447 688	21
g_S/g_P'	658.227 59	22

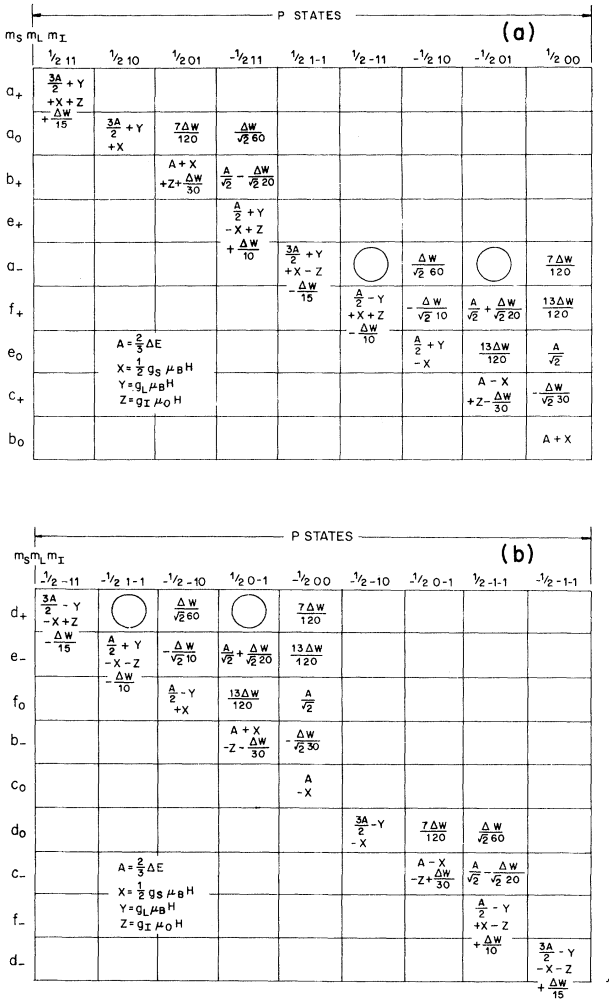

FIG. 3. Zeeman plus spin Hamiltonian for the $n = 2$ state of $^6Li^{2+}$ in the (L, m_L, m_S, m_I) representation. The matrix is symmetric about the diagonal and only the upper half is shown.

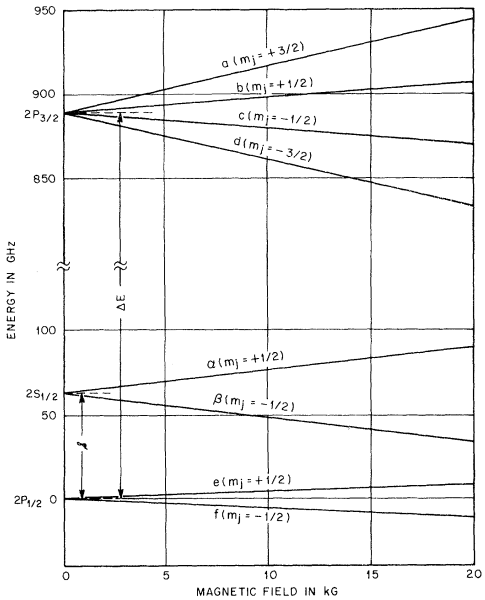

FIG. 4. Zeeman energy levels for the $n=2$ state of $^6Li^{2+}$. The labels are used in the text as abbreviations for the sublevels, following the usage of Lamb and Retherford (Ref. 13).

pole-matrix elements, which allows construction of a precision curve-fitting formula and extraction of the zero-field Lamb shift. To achieve this goal the following procedure was used. An effective Zeeman Hamiltonian was written for both S and P states. A Hamiltonian matrix was evaluated using

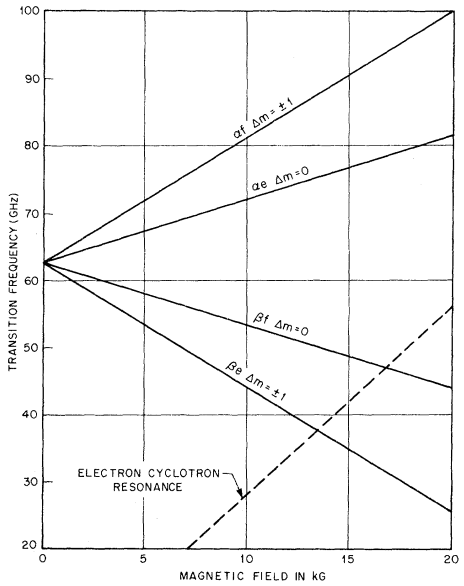

FIG. 5. Relevant transition frequencies for the $n=2$ state of $^6Li^{2+}$. The dashed line shows the electron cyclotron frequency. Transitions with $\Delta m=\pm 1$ require perpendicular polarization, whereas $\Delta m=0$ transitions require parallel polarization.

the "high-field" $(L, m_L m_S m_I)$ representation. The complete 24×24 matrix was then computer diagonalized to obtain eigenvectors as well as eigenvalues. The eigenvectors were used to calculate the dipole-matrix elements from a knowledge of their values in the $L, m_L m_S m_I$ representation,[14] and all eigenvalues and matrix elements were stored for later use in curve fitting.

The effective Hamiltonian is obtained from that given by Lamb[15] for the $n=2$ state of hydrogen. For our S states it is

$$\mathcal{H}_{2S}=\mathcal{S}+g_S\mu_B\vec{S}\cdot\vec{H}+\tfrac{2}{3}\Delta W\vec{I}\cdot\vec{S}+g_I\mu_B\vec{I}\cdot\vec{H}, \tag{2}$$

while for P states

$$\mathcal{H}_{2P}=\tfrac{2}{3}\Delta E+\tfrac{2}{3}\Delta E\,\vec{L}\cdot\vec{S}+g_S\mu_B\vec{H}\cdot\vec{S}+g_L\mu_B\vec{H}\cdot\vec{L}$$
$$+g_I\mu_B\vec{H}\cdot\vec{I}+\tfrac{1}{24}\Delta W\{2\vec{I}\cdot\vec{L}+\tfrac{2}{5}[4\vec{I}\cdot\vec{S}-3(\vec{I}\cdot\vec{L}\vec{L}\cdot\vec{S}$$
$$+\vec{L}\cdot\vec{S}\vec{I}\cdot\vec{L})]\}. \tag{3}$$

The zero of energy has been taken at the $2P_{1/2}$ level and the convention that g_S and g_L are positive numbers and g_I is a negative number has been adopted. Table II lists the employed g values in units of Bohr magnetons. In Fig. 3 the "high-field" representation of the effective Hamiltonian is shown. Off-diagonal elements arise from the hyperfine and spin-orbit interactions and cause mixing of the basis vectors. The energy levels and transition frequencies derived from a diagonalization of this matrix are shown in Figs. 4 and 5. The labels α and β and $a,\ldots,f$ are used as abbreviations for the sublevels, following the usage of Lamb and Retherford.[13] Each of the high-field sublevels is in fact a triplet corresponding to the three orientations of the nuclear spin $(I=1)$ in the magnetic field H, but are unresolved on the scale of Fig. 4.

Since the experimentally measured quantities are the frequency of an atomic transition instead of an energy difference and proton resonance frequencies instead of magnetic fields, there is an advantage in precision if all energies are expressed as frequencies, and the magnetic-field-dependent terms of the Hamiltonian are calculated directly from the measured resonance frequency ν_{NMR} of protons in water. This is done using the relationship

$$\nu_{\mathrm{NMR}}=g_P'\mu_B H/h \tag{4}$$

and the known ratio g_S/g_P' of the free-electron spin-g value to that of the proton in water. Thus the magnetic-field-dependent terms have been written as

$$g_S\mu_B H/h=(g_S/g_P')\nu_{\mathrm{NMR}},$$
$$g_L\mu_B H/h=(g_S/g_P')(g_L/g_S)\nu_{\mathrm{NMR}}, \tag{5}$$
$$g_I\mu_B H/h=(g_I/g_S)(g_S/g_P')\nu_{\mathrm{NMR}},$$

throughout the course of the analysis.

IV. APPARATUS

A. Magnetic field

The magnetic field was provided by a 15-in. iron-core Varian Model V3800 electromagnet with pole pieces tapered to 8.56 in. and a gap of 3.08 in. Its power supply (Varian Model VFR2703) uses a Hall-effect device in a feedback circuit to maintain the field at a value determined by the setting of a reference voltage. In operation field drifts of <0.1 G/h were observed. The homogeneity of the field over the volume of the electron beam is also <0.1 G as measured by a movable NMR probe. Since the slope of the microwave transition frequency under study is of the order of 2 MHz/G (see Fig. 5), no corrections were made for field stability or homogeneity as they would shift the result by <0.2 MHz.

B. Magnetic field measurement

A Magnion model G-502 NMR gaussmeter modified to allow low modulation amplitude was used for field measurements. The probe was situated outside the vacuum envelope but only 1.17 in. from the interaction region. Measurements indicated that field at the probe site was about 0.1 G lower than the field at the electron beam; hence no correction was made for probe position.

Because of the relatively large magnetic fields employed in this experiment it was found convenient to use a deuterated-water sample for making the NMR measurements. This keeps the NMR frequencies within the range of the Magnion marginal oscillator at the highest fields employed. The measured deuteron NMR frequencies were then converted to proton NMR frequencies using the published conversion factor[23] of (42.577/6.5357). As a check the ratio of proton and deuteron NMR frequencies was measured in the same probe at lower magnetic fields where both resonances could be observed. No deviation from the published ratio was found.

C. Vacuum system

An all-metal and metal-seal vacuum chamber was fabricated predominantly from stainless steel and pumped on by a Welch Model 3103 turbomolecular pump and an NRC Model 206 Orb-Ion pump operating in parallel. The part of the envelope that fit between the pole pieces of the magnet and contained the interaction region was fabricated from a unique alloy of columbium and tantalum, Fansteel 80. The multiple restrictions of needing a material resistant to lithium attack, of low magnetic susceptibility and of good vacuum properties, led us to this unusual material. The base pressure in the fully loaded system after bake-out was about 1×10^{-7} Torr. The pressure was measured with a Varian Model UHV-24 ionization gauge and Varian Model MIC-10 mTorr gauge situated close to the interaction region but outside of the magnetic field. All of the experimental components aside from the soft-x-ray detection system were mounted on a single flange which was sealed to the top of the Fansteel 80 chamber via a gold corner seal. Since a considerable amount of recycling was anticipated, the entire vacuum system was mounted on a track and could be hand cranked in and out of the magnet. The residual gas in the chamber was analyzed with a Varian model 974-0036 partial-pressure gauge and showed mainly water vapor and air.

D. Soft-x-ray detection system

A windowless Bendix Model M-306 crossed-field photomultiplier faced the IR along a horizontal axis perpendicular to the magnetic field. The 0.62-in. by 0.72-in. tungsten photocathode of this detector was vacuum coated with a 3000-Å layer of LiF to enhance its quantum efficiency in the soft-x-ray region.[24] Because the large magnetic field in the IR would seriously disturb its operation, the photomultiplier was removed 26 in. off axis and coupled to the IR via a light pipe. The light pipe consisted of a hollow glass tube 24 in. long with a $1\frac{5}{8}$-in. i.d. which had been flashed internally with gold. A 2500-Å-thick 0.62-in.-diam Be filter provided by Penn Spectra-Tech was hermetically sealed onto the photomultiplier end of the light pipe. The transmission properties of this film[25] were such as to make it an ideal pass filter for 135-Å radiation. A small hole was made in the Bendix end of the light pipe which allowed the injection of gas at high pressure that subsequently flowed down the light pipe and on to the pumps. To maximize the pressure differential between the inside of the light pipe and the IR, a gas baffle was placed at the end of the light pipe. This consisted of ten circular disks $1\frac{5}{8}$ in. in diameter by 0.01 in. thick separated by 0.125 in. Each disk contained a rectangular hole 0.75 in. by 1.00 in. aligned parallel to the electron beam. It was hoped that this baffle would create a turbulent flow pattern at the exit of the light pipe and reduce its conductance.

E. Lithium oven and lithium

The lithium oven was an end-loaded molybdenum cylinder 3.5 in. long by 1.5 in. in diameter situated within a double layer of tantalum heat shield. The lithium exited through a 0.715-in. diam by 0.265-in.-thick tungsten crinkle-foil nozzle located 0.6 in. below the electron beam. Heat was provided to the oven by means of a bifilar heater wrapped

around the nozzle. This ensured that the nozzle would be the hottest part of the system and would not clog. Also, the bifilar nature of the heater reduced the stray magnetic fields to negligible proportions. The ^{6}Li was obtained in metallic form from Oak Ridge National Laboratories and is 99.3% isotopically pure. Since the $^6Li^{2+}$ and $^7Li^{2+}$ Lamb shifts are identical to the accuracy of this experiment no correction has been made for the 0.7% contamination with ^{7}Li. Twenty-two gram ingots of ^{6}Li were prepared for us by the Lithium Corporation of America and the oven was loaded with one ingot at a time. Finally, the oven temperature was monitored by a thermocouple mounted on its side.

F. Interaction region

At the heart of the IR is a rectangular field-free drift space maintained at ground potential (see Fig. 6). Ions and electrons can enter or leave this region along the magnetic field lines through two 90%-transparent grids. The IR is bounded from below by the nozzle of the lithium oven and from above by the microwave horn, whose final dimensions are similar to those of the drift region. Electron flow into the region is initiated by running the cathode potential below ground. The cathode is a matrix type with a 0.5-in. diam with a potted bifilar heater. A simple form of ion trapping is achieved by running the collector and grid potentials slightly positive with respect to ground. When ions produced in the drift region with a fraction of a volt of kinetic energy attempt to leave along the field lines they are driven back in by these reflector voltages. Key elements in the IR have been shielded and

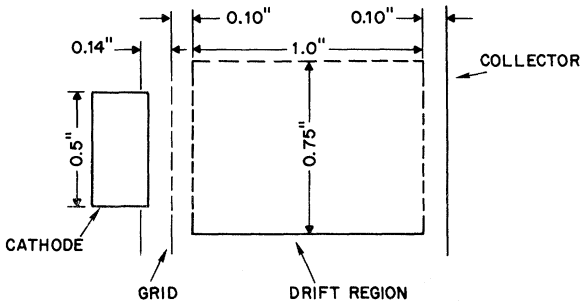

FIG. 6. Top view of the interaction region.

heated to about 500 °C to reevaporate deposited Li and prevent shorts. Light emanating from the entire IR is viewed by the light-pipe system through a 93%-transparent grid.

G. Microwave system

A schematic diagram of the microwave system is given in Fig. 7. About 10 W of power at 35.8 GHz was provided continuously by a Varian Model VKA 7010C two-cavity Klystron. The power is delivered to the system in pulses by a Microwave Associates Model 8314-1Q3 diode switch. Measurement of the output-power stability of the system indicated that that power leveling would be necessary. Hence the output waveform was sampled with a Hewlet-Packard Model 422A crystal detector and the average power maintained constant to about 0.1% with the aid of a Ferrotech Model 305LS variable attenuator. Measurement of the output frequency was made directly with a Systron-Donner Model 1017

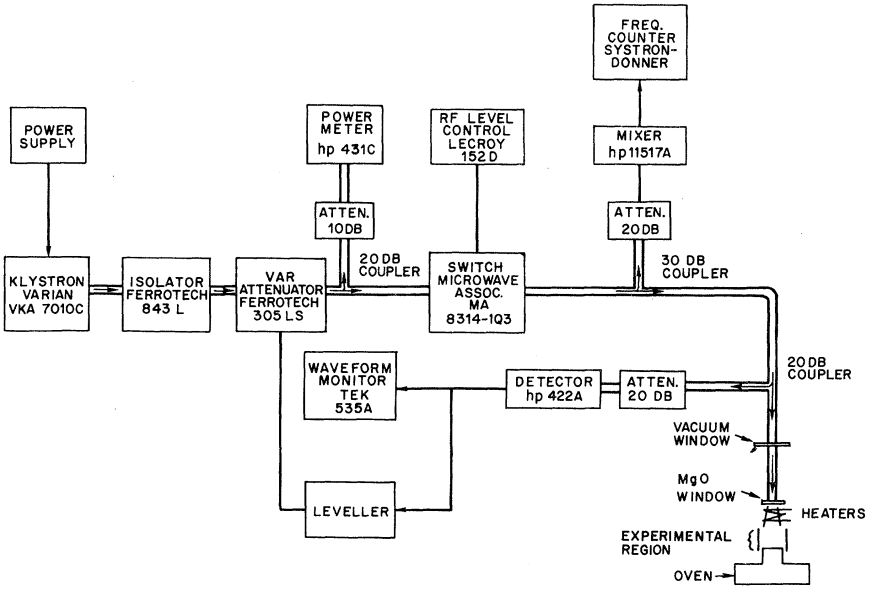

FIG. 7. Block diagram of the microwave system.

frequency counter and Model 1298 transfer oscillator plug-in calibrated against the frequency broadcast by station WWV. Since frequency drifts of only about 1 MHz/h were observed, this was deemed acceptable and no attempt was made to phase lock the Klystron. Finally, the power entered the IR through a 10^{-2}-in. MgO window and a homebuilt tantalum microwave horn wrapped with bifilar heaters and maintained at 540 °C, which served to keep the microwave transmission system lithium free. The output dimensions of the horn were 0.81 in. by 0.56 in. and it was located 0.5 in. above the center of the electron beam with its longer dimension parallel to it.

V. PRELIMINARY OBSERVATIONS

A. Signal strength

Assuming that all metastables are trapped and eventually undergo an rf transition, the estimated number of induced counts per bombardment pulse is given by

$$n = \tfrac{1}{2}\sigma^{2+}(2S)(I/e)l\delta T\eta_G\eta_K\eta_B\eta_W Q\omega G, \qquad (6)$$

where $\sigma^{2+}(2S)$ is the cross section for double ionization and excitation to the $2S_{1/2}$ state by 650 eV electrons, I is the bombardment current, e is the electronic charge, l is the observed length of the IR, δ is the lithium-atom density in the IR, T is the time duration of the e-gun pulse, η_G is the transmission of the viewing grid on the IR, η_K is the transmission of the krypton gas in the light pipe, η_B is the transmission of the Be film and mount, Q is the quantum yield of the photocathode, ω is the fraction of the total 4π solid angle subtended by the photocathode at the IR, η_W is the transmission of the entrance grid to the photomultiplier, and G is the light-pipe "gain." The uncertainties associated with several of the quantities in Eq. (6), in particular $\sigma^{2+}(2S)$, δ, Q, and G, are such that the evaluation of n must be taken only as a crude order-of-magnitude estimate to be compared with the observed value of about 2×10^{-3} high-microwave-power-induced counts per bombardment. The total double-ionization cross section σ_T^{2+} has, to our knowledge, never been measured or calculated—much less the cross section for population of a particular atomic state. Following the procedure of Lamb and Skinner[26] we have made a sudden-approximation calculation which indicates that about 1% of the doubly ionized lithium atoms should be in the $2S$ state. While not performing an actual calculation of σ_T^{2+}, Wu and Yu[27] have estimated a value of $\sim10^{-18}$ cm^2. Hence a value of $\sigma^{2+}(2S)\sim10^{-20}$ cm^2 is probably reasonable. Typical values for the other parameters are $I = 9$ mA, $l = 2.5$ cm, $\delta = 3\times10^{11}$ atoms/cm^3, $T = 6$ μsec, $\eta_G = 0.93$, $\eta_K = 0.75$, $\eta_B = 0.45$, $\eta_W = 0.90$, $Q = 0.3$, $\omega = 5.3\times10^{-5}$, and $G = 5$. Using these values a value for n of 3×10^{-2} microwave-induced counts per bombardment is calculated. In view of the uncertainties involved this does not appear to be in too great disagreement with observation.

B. Excitation curve

In Fig. 8 the relevant energy levels of the lithium atomic and ionic species are indicated. Clearly a real microwave signal should have an onset in the vicinity of 173 eV. In Fig. 9 a plot of the microwave-induced signal as a function of bombardment voltage is presented. This curve, with its apparent threshold in the proper region, was obtained at an early stage of the experiment and convinced us that the feeble resonances being observed at the time were indeed the sought-after result. Most of the precision data were taken at a bombardment voltage of 650 eV, well beyond the peak in the excitation curve, so as to maximize the signal-to-noise ratio.

C. Microwave quenching curve

The induced microwave transition probability per unit time may be written as[13]

$$\mu_i = \frac{2\pi e^2 S_0}{c\hbar^2\tau_{2P}} \frac{|X_i|^2}{(\omega_0-\omega_i)^2+(1/2\tau_{2P})^2}, \qquad (7)$$

where S_0 is the incident-energy flux density at circular frequency ω_0 and X_i and ω_i are the matrix element of the coordinate vector and level splitting for a particular hyperfine component of the βe transition in the applied field. If it is assumed that

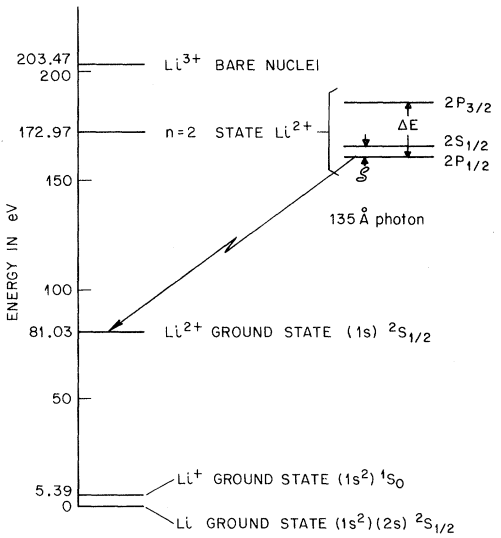

FIG. 8. Relevant energy levels of the lithium atomic and ionic species.

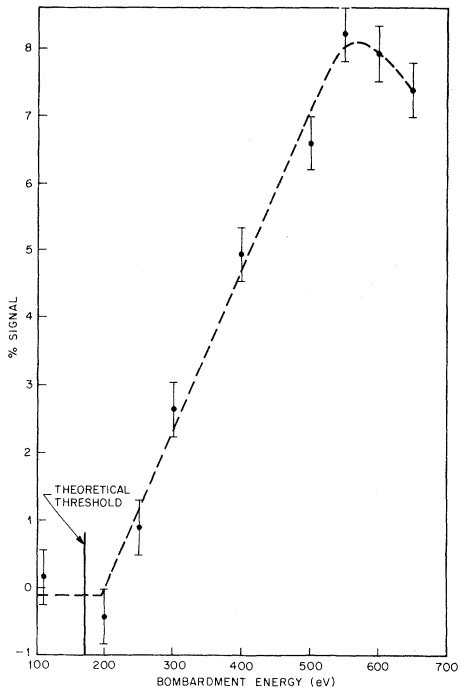

FIG. 9. Excitation curve showing the dependence of the microwave induced signal on electron bombardment voltage. In the final version of the apparatus this curve peaked at a signal value of ~35% for 6.0 W of microwave power.

the metastables remained trapped for the full duration of the microwave pulse ($t = 4\ \mu$sec), then the fraction of them quenched by the microwaves is

$$\varphi_i = 1 - e^{-\mu_i t} . \tag{8}$$

At resonance $\omega = \omega_0$ and the power required to produce 63% quenching is defined by the relation

$$\mu_i(\omega = \omega_0)t = 1 . \tag{9}$$

Solving this equation for S_0 and employing a value of $|X_i|^2 = 0.34a_0^2$ obtained by computer diagonalization yields $S_0 = 0.77$ W/cm^2. Since the output area of the microwave horn sitting directly above the metastable beam is 2.9 cm^2, this calculation predicts that about 2.2 W must be delivered to the interaction region to produce 63% saturation of the transition. Here plane-wave propagation with no cavity effects has been assumed. As can be seen from Fig. 10, the transition appears to saturate at a value that is compatable with this prediction though somewhat higher. Microwave attenuation in the MgO window and divergence of the microwave beam could easily account for this effect. Equation (8) also predicts a characteristic shape for the saturation curve. The theoretical curve of Fig. 10 represents a fit of this theoretical expression to the data with 100% quenching taken at 28 units and 63% quenching occurring at 3.2 W. The reasonable

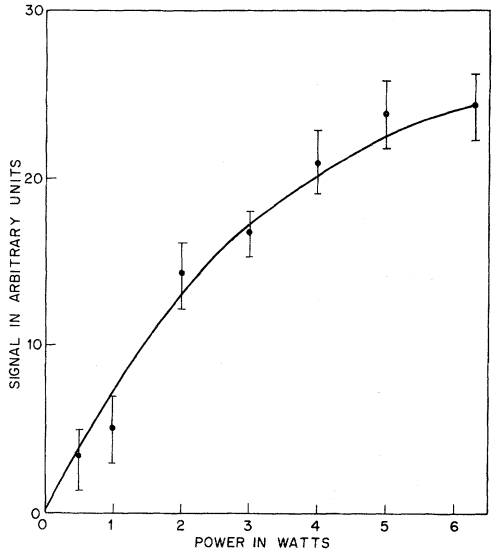

FIG. 10. Microwave saturation curve. The solid line is a theoretical curve discussed in the text.

agreement with the data encourages the belief that the basic microwave quenching process is under control.

D. Ion trapping

Ion trapping was undertaken for two basic reasons: (i) to enhance an extremely feeble signal,

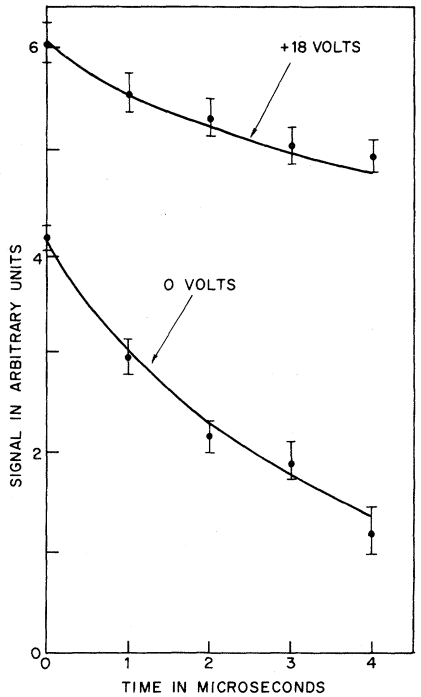

FIG. 11. Study of the effectiveness of the ion trapping. Time is measured from the beginning of the normal scaler gate.

and (ii) to ensure containment of the metastables for the duration of the microwave pulse and thus greatly simplify the theoretical line shape employed in computer curve fitting (see Sec. VI). Since containment for a period of at most 11 μsec was desired, an extremely simple trap was employed, as discussed above. Observation of the trap's effectiveness indicated that it was adequate for our purposes. Turning up the reflector potential from 0 to 18 eV increased the signal by a factor of 2. The effective containment time was determined by a series of measurements made with a movable microwave gate. Data were taken as a 1-μsec-long microwave pulse and coincident scaler gates were moved out from the beginning of the normal 4-μsec scaler gate. Each point is therefore a measure of the number of metastables in the trap at that time. Curves taken for two different values of the reflector potential are shown in Fig. 11. A large improvement in containment time with trapping voltage is apparent; i.e., if we consider the time required for the metastable population to decrease by, say, 20%, this number has increased from about 1 to 4 μsec. Further increase in the trapping voltage beyond 18 eV did not improve the containment. The residual decrease in signal at 18 eV is probably due to a combination of leakage from the trap and other quenching mechanisms to be discussed later.

E. Electron cyclotron resonance

It is apparent from Fig. 5 that the electron cyclotron resonance is a potentially dangerous interloping phenomenon. If stray electrons in or near the IR are accelerated by the microwave fields at resonance and then collide with gas atoms or walls to make soft-x-ray photons (~100 to 300 eV) a serious distortion of the Lamb-shift resonance could result. In fact, this is exactly what happened in an earlier version of the apparatus. At that time the microwave power was being brought in horizontally and collinear with the optical detection system. The problem was solved by bringing the microwave power in from above. When the photomultiplier could no longer see into the microwave horn and transmission line, the cyclotron resonance disappeared. Calculations indicate that only the very intense fields inside the microwave horn are large enough to produce this effect.

F. Krypton gas

The lifetime of the soft-x-ray detection system was extended from about 1 to 10 h by flowing a small amount of research-grade krypton gas down the light pipe. Evidently only about one in ten of the lithium atoms which would normally condense on the light pipe and Be filter could do so when the krypton was flowing. The restrictions on what gas could be used were numerous. The gas could not poison the cathode, react with the lithium, produce soft x rays upon electron bombardment, or absorb 135-Å photons excessively. After experimenting with many gases krypton was chosen. The krypton flow rate used for most of the data acquisition resulted in a pressure of 2×10^{-6} Torr near the IR. With this much krypton in the system an increase of 15% in the background counts and a decrease of 25% in the microwave signal was observed. Evidence that the decrease in microwave signal was due to photon absorption by the krypton was obtained by injecting the gas into the IR from outside the light pipe. A greatly reduced attenuation was observed. An experiment was performed to determine if any microwave effect on the counting rate could be observed with only krypton in the chamber; it yielded a null result.

VI. METASTABLE QUENCHING AND REMOVAL PROCESSES

A. Metastable velocity

Precision data were taken with an oven temperature T_0 that varied between 475 and 550 °C. For the purpose of this estimate we assume a fixed value of $T_0 = 527$ °C corresponding to 800 °K. The thermal velocity V is then given by $(3kT_0/M)^{1/2}$, where k is the Boltzmann constant and M is the mass of ^{6}Li. Evaluation of this expression yields $V = 1.82\times10^5$ cm/sec, corresponding to a thermal energy of 1.03×10^{-1} eV.

Besides the thermal velocity an additional recoil component of velocity is given to the metastables upon formation. This is estimated by assuming that two electrons are suddenly removed from their orbits around the Li nucleus, which must then recoil to take up the momentum characteristic of these bound electrons. In the usual way[9] the recoil velocity V_R is estimated as

$$V_R = (m/M)\alpha c(Z_{1S}^2 + Z_{2S}^2)^{1/2}, \tag{10}$$

where Z_{1S} and Z_{2S} are effective nuclear charges seen by electrons moving in partially screened hydrogenic orbits about the Li nucleus. Employing the values $Z_{1S} = 2.61$ and $Z_{2S} = 1.40$ provided by Carlson *et al.*[28] yields $V_R = 5.92\times10^4$ cm/sec, corresponding to an energy of 1.09×10^{-2} eV.

Finally, for the purpose at hand it is accurate enough to add the thermal and recoil energies to obtain a total energy of 1.14×10^{-1} eV. Assuming an isotropic velocity distribution, this yields a longitudinal component of velocity $V_Z = 1.10\times10^5$ cm/sec and a transverse component of velocity $V_T = 1.55\times10^5$ cm/sec in the IR. These numbers will be used in the discussion to follow.

B. Atom and ion densities

To estimate the atom density in the IR one must have a reasonable understanding of the lithium-atom flow rate N through the crinkle-foil nozzle. Fortunately, this problem has been studied in considerable detail by Lucatorto[29] and Giordmaine and Wang.[30] They have shown that a reasonable representation of N for our flow conditions is given by

$$N=\tfrac{2}{3}\pi(n_0 V r^3 D/L), \tag{11}$$

where n_0 is the Li-atom number density in the source, r is the effective hole radius, V is the atom velocity, L is the hole length, and D is the total number of holes in the nozzle. Typical values of these parameters are $n_0=1.2\times10^{14}$ atoms/cm^3, $V=1.82\times10^5$ cm/sec, $r=2.7\times10^{-3}$ cm, $L=0.67$ cm, and $D=4.7\times10^4$ holes, which yield a value of $N=6.3\times10^{16}$ atoms/sec upon introduction into Eq. (11). The values of r and D were taken from the work of Giordmaine and Wang,[30] since both nozzles were produced by the same process at Columbia University. Since the area of the nozzle is 2.5 cm^2 this gives an atomic current density of $\rho=2.5\times10^{16}$ atoms/cm^2 sec emitted from the nozzle. If these atoms were emitted in a highly collimated beam moving with their average thermal velocity, the atom density δ in the IR directly above the nozzle would be defined by the relation

$$\rho=\delta V, \tag{12}$$

which gives $\delta=1.4\times10^{11}$ atoms/cm^3. Here any containment of the atoms in the IR has been ignored. However, an observer sitting at the center of the IR and looking about would see a complicated ~40%-transparent surface made up predominantly of hot molybdenum and tantalum. If it is assumed that each atom after striking an IR surface is reevaporated at a random angle, this means that a typical atom will pass through the IR ~2 times before leaving. Thus we take $\delta\approx3\times10^{11}$ atoms/cm^3 as a characteristic value.

Of interest when considering possible space-charge effects is the Li-ion density δ^+ in the IR during the microwave on-time. This may be obtained from the expression

$$\delta^+=\sigma_T^+(I/e)(\delta/A)T, \tag{13}$$

where it is assumed that all ions produced during the e-gun on-time of $T=6$ μsec remain trapped within the electron beam volume, σ_T^+ is the total single-ionization cross section,[31] and A is the area of the electron beam. Taking typical values of $\delta=3\times10^{11}$ atoms/cm^3, $I=9$ mA, $\sigma_T^+=8\times10^{-17}$ cm^2, and $A=1.27$ cm^2 yields $\delta^+=6.4\times10^6$ Li$^+$ ions/cm^3.

C. Motional Stark quenching

Because of the component of metastable velocity transverse to the applied magnetic field H, a "motional" electric field E_m is generated in the rest frame of the ion. This field is in a direction normal to H and of magnitude

$$E_m=(1/c)V_T H. \tag{14}$$

At the resonance center $H_0\approx14.4$ kG and, taking $V_T=1.55\times10^5$ cm/sec, Eq. (14) gives $E_m=22.3$ V/cm. Metastables will be quenched exponentially by this field at a rate $\gamma_i=1/\tau_i$, given by[32]

$$\frac{1}{\tau_i}=\frac{e^2E_m^2|X_i|^2}{\hbar^2\tau_{2P}[\omega_i^2+(1/2\tau_{2P})^2]}, \tag{15}$$

where X_i is the matrix element of the coordinate vector between a particular β sublevel and e sublevel with the same m_I and ω_i is the splitting between them in circular frequency units. Quenching via more distant P states is negligible and has been ignored in Eq. (15). Evaluation of Eq. (15) at the resonance center yields $\tau_i=91.9$ μsec. Thus about 4% of the metastables should be motionally quenched during the 4-μsec microwave gate period.

D. Space-charge quenching

Because of their comparatively large velocity and energy it is expected that most of the primary and secondary electrons will have left the IR during the 1-μsec delay after the e-gun pulse.[9] There remains, however, a Li$^+$-ion density δ^+ calculated above. Macroscopic electric fields associated with this space-charge density could conceivably result in significant quenching. If the length of the space-charge column is assumed to be long with respect to its radius, end effects can be neglected and a radial field of maximum magnitude

$$E_S=2\pi R\delta^+ e \tag{16}$$

is obtained at the outer edge of the column from a simple electrostatics calculation. Inserting values for the radius $R=0.64$ cm and $\delta^+=6.4\times10^6$ Li$^+$ ions/cm^3 into Eq. (16) yields a maximum value of $E_S=3.7$ V/cm. The average radial field over the cross section of the column is about half this value. Since this field is quite small with respect to the motional electric field, which itself does minimal quenching, effects associated with E_S have been ignored. It can also be shown by making an elaborate electrostatics calculation that longitudinal electric fields, associated with the fact that the beam is of finite length, are of the same magnitude but somewhat smaller than the radial fields. These have likewise been neglected in considering quenching effects.

E. Wire collision quenching

To ensure that the trapping fields do not penetrate into the IR, 90%-transparent grounded grids were placed over the entrance and exit. Metastables colliding with these wires would surely be quenched. Since the longitudinal velocity is 1.1×10^5 cm/sec and the interaction region is about 2.5 cm long, typically 18% of the metastables will pass back and forth through a grid during the 4-μsec-long microwave pulse resulting in a net quenching of about 4%.

F. Stark quenching in reflector field

As indicated above, about 18% of the metastables will pass through the trapping field during the microwave on time. Assuming plane parallel geometry these metastables will experience a uniform reflector field E_R of 70.9 V/cm. According to Eq. (15) the metastables should decay exponentially in this field with a lifetime of 9.1 μsec. From simple one-dimensional Newtonian mechanics the time spent in the reflector field, T_R, is given by

$$T_R = 2MV_z/eE_R . \tag{17}$$

Evaluation of Eq. (17) yields $T_R = 1.9\times10^{-2}$ μsec. Thus the Stark quenching which occurs in the reflector fields is negligible.

G. Spontaneous decay

The metastables are decaying spontaneously by a two-photon process with a lifetime of 167 μsec. Hence over the course of the 4-μsec-long microwave gate period about 2% of the population will have decayed by this process.

H. Gas collision quenching

Metastable ions can be quenched in a gas collision process with the lithium atoms of density $\delta = 3\times10^{11}$ atoms/cm^3 always present in the IR. The mean free time between such collision, τ_c, can be written as

$$\tau_c = 1/\delta\sigma_c V , \tag{18}$$

where V is the ion velocity taken as 1.9×10^5 cm/sec and σ_c is the cross section for the quenching process. While σ_c is unknown, an order-of-magnitude estimate of τ_c can be made by employing the cross section for a similar process, i.e., He^+ metastable quenching on He atoms. Lipworth and Novick[1] report an unpublished estimate for this cross section of $\sim4\times10^{-15}$ cm^2 at atomic velocities comparable to the present case. Employing this value yields $\tau_c = 4400$ μsec. Hence, most likely, collisional quenching is not an important effect in this experiment. Additional support for this belief comes from the fact that it is difficult to imagine why this process would be dependent on the hyperfine sublevel which the metastable is in. In Sec. VII it is shown that quenching processes which are independent of the hyperfine sublevel can be ignored in the fitting without shifting the result.

VII. LINE SHAPE AND NORMALIZATION

A basic simplifying assumption underlying the line-shape theory presented here is that all the metastables remain trapped for the full microwave gate period and experience the same microwave electric field during this interval. In practice some departure from this assumption was observed. As can be seen from Fig. 11, about 18% of the metastables have been removed from the IR or quenched during the 4-μsec gate period. On the basis of the discussion in Sec. VI a 10% figure can be understood in terms of a combination of motional Stark quenching, wire collision quenching, and spontaneous decay. This leaves 8% unaccounted for. Most likely this is due to residual ion leakage out of the trap because of lateral motion induced by the space-charge fields.[9] Because of the normalization procedure employed in the data acquisition sequence, ignoring this effect will produce no shift in the line center. Indeed, it is shown below that any quenching or removal process which affects all the magnetic sublevels equally can be ignored in the line-shape formula.

Assuming that all quenching processes are independent, that μ_i is the probability per unit time that a particular metastable hyperfine component is quenched by the microwaves [see Eq. (7)], and that λ_i is the probability per unit time for quenching by any other process, the number of counts C detected during the scaler gate time is

$$C = \sum_{i=1}^{3} \epsilon N_i e^{-\lambda_i t}(1 - e^{-\mu_i t}) + B , \tag{19}$$

where ϵ is the over-all efficiency for detecting 135-Å photons, N_i is the number of metastables present in the IR at the beginning of the gate period, and B is the detected number of background counts which have nothing to do with metastable quenching. Since ϵ, N_i, and B are all expected to vary significantly with magnetic field and time in an undetermined fashion, a normalization procedure which removes these quantities from the final signal expression is essential. As described in Sec. II, data were taken sequentially for three different microwave power levels: first low power, then high, and finally with the microwaves off. The signal is then defined as

normalized signal

$$= \frac{\text{scaler 1 counts} - \text{scaler 3 counts}}{\text{scaler 2 counts} - \text{scaler 3 counts}} . \tag{20}$$

Substituting Eq. (19) into Eq. (20) then gives

$$\text{normalized signal} = \frac{\sum_{i=1}^{3} e^{-\lambda_i t}(1 - e^{-\mu_i^L t})}{\sum_{i=1}^{3} e^{-\lambda_i t}(1 - e^{-\mu_i^H t})} , \tag{21}$$

since by definition ϵ, N_i, and B are quantities that are independent of microwave power and N_i may be assumed equal for the three hyperfine states. In practice the ability to utilize a normalization procedure like the one outlined above depends heavily on being able to appreciably saturate and broaden the resonance at the high-power level. If this is not the case, the resonance will disappear after performing the division indicated in Eq. (20). In any event a dear price must be paid for the scheme, since much time is lost by taking resonance data at two power levels, and many potential microwave-induced counts are sacrificed at the low-power level. However, in this experiment such a normalization scheme was essential and it was employed. Fortunately, a high-quality result was still attainable.

The form of the μ_i used in curve fitting is given by Eq. (7). This expression allows for microwave-induced transitions between two specific hyperfine sublevels of the β and e states. In actuality, the microwaves may also induce transitions between the β state and other $2P$ sublevels in an off-resonant fashion. The tails of these "overlapping" resonances could in principle shift the observed center of the primary βe resonance. Computer studies indicated that only the nearest overlapping transition, βf, was a serious problem. It was allowed for in the fitting by taking each μ_i as a sum of two similar terms, one for βe and one for βf. A problem arose here in that βf is driven by microwaves of polarization opposite to βe. If the microwave transmission system were in fact perfect, the βf transition would not be observable in our apparatus because the microwaves are ostensibly delivered to the IR polarized perpendicular to the magnetic field. The relative amounts of parallel and perpendicular polarization actually present in the IR were determined by experiments with He^+. For this ion Lamb-shift transitions of both polarization could be observed simultaneously. In this way it was found that the ratio of perpendicular polarized power to parallel polarized power was very close to 10. Thus when summing the two components of each μ_i the βf component was reduced by a factor of 10. Inclusion of the βf transition in the fitting was observed to shift the result on the order of 10 MHz.

A study of the form of Eq. (21) leads to the welcome conclusion that all quenching and removal processes contained in λ_i, which affect the different hyperfine levels equally, are not present in the final normalized signal expression. It is believed that the only process of significance not removed by this normalization scheme is Stark quenching by the motional electric field. Because of the slight displacement of the hyperfine levels the Stark quenching rate will be slightly different for each of the sublevels in a given magnetic field. This effect is allowed for in the fitting by taking $\lambda_i = 1/\tau_i$, as given by Eqs. (14) and (15). The inclusion of motional Stark quenching in the line shape was observed to shift the result by a few MHz.

Finally, a brief mention of possible Stark shifts is appropriate at this point. Besides quenching the metastables and distorting the line shape, electric fields will produce direct Stark shifts of the line centers. Conceivably a correction for this effect could be made in the line-shape expression. However, a straightforward calculation[14] indicates that in electric fields of the order of tens of V/cm the resulting shifts are only a small fraction of a MHz. Hence it is possible to ignore this effect in the present experiment.

VIII. PROCEDURE

After chemically cleaning the apparatus the oven was loaded with lithium and the system pumped down for several days. A base pressure in the 10^{-8}–10^{-7}-Torr region was usually achievable after this period. System bake-out then commenced as the oven and various heated components were slowly brought up to temperature. After 1–2 days, when the base pressure of the hot system approached 1×10^{-7} Torr, data acquisition began. All of the electronics including the magnetic field were turned on and allowed to stabilize for several hours. An official run began with the setting and recording of all experimental parameters. Next the microwave frequency was measured and recorded. The magnetic field was then stepped to the first of 14 data acquisition points and counts were recorded for a 4-min interval. During this interval the magnetic field was measured with the NMR system. After completion of the 4-min interval the counts were recorded as the field was stepped to a point on the other side of the resonance. In this fashion data were taken at all 14 field points on alternate sides of the resonance center. A run was deemed complete when some arbitrarily selected number of low-microwave-power-induced counts (~15 000) had been recorded at the resonance center. Gen-

TABLE III. Experimental parameters and data from a standard run.

Microwave Frequency at start	35 795.9 MHz
Microwave frequency at finish	35 796.7 MHz
Electron-gun current	9 mA
Electron-gun voltage	−650 eV
Oven temperature	475–485 °C
Krypton pressure	2×10^{-6} Torr
Low microwave power	1.5 W
High microwave power	6.0 W
Horn temperature	540 °C
Reflector voltage	+18 eV

NMR (MHz)	Low-power counts	High-power counts	Background counts
10.0322	143 380	180 003	128 314
5.7700	93 945	105 587	90 587
8.2170	121 229	152 146	110 262
6.7769	103 505	119 925	99 464
11.8746	126 183	140 351	122 358
7.2541	102 536	120 870	97 303
9.3917	128 481	164 248	112 915
7.7363	104 465	128 009	96 981
11.4996	123 786	140 101	118 993
8.6058	108 531	139 222	96 763
11.1639	115 393	134 082	110 049
10.3630	115 752	143 294	106 465
8.8999	113 897	145 296	101 971
10.6869	104 567	126 630	97 164

erally two or three cycles through the 14 points were adequate to give this number of counts. Since the magnetic fields were resettable to a fraction of a G, data from successive 4-min intervals were added together and the field measurements averaged. At the completion of a run the microwave frequency was again recorded. Data from a standard run are presented in Table III and illustrated in Fig. 12. These data, which were obtained in two cycles, are adequate to determine $\mathcal{S}$ to a statistical accuracy of about ±200 MHz and yielded explicitly $\mathcal{S} = 62\,444$ MHZ.

At the completion of a run the experimental parameters were changed to those desired for the

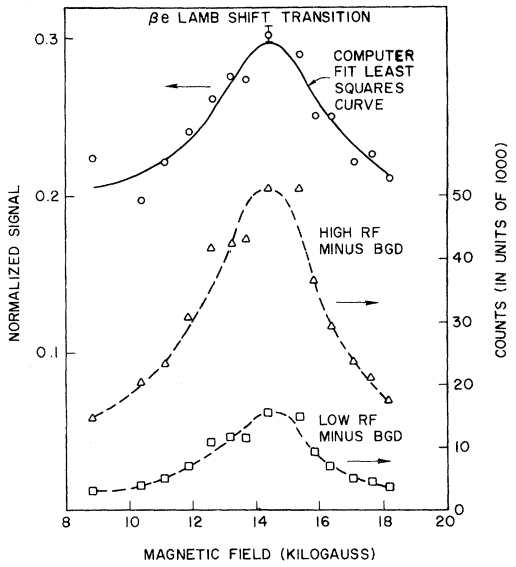

FIG. 12. Typical resonance curve. The actual data and experimental parameters for this run are given in Table III.

next run and data acquisition again commenced. In this way resonance data were taken as the parameters were varied in a methodical way. In general over the course of a single run the data acquisition rate was observed to decrease visibly because of lithium accumulation in the soft-x-ray detection system. To compensate for this effect the oven temperature, which started at about 475 °C for a clean system, was gradually raised to keep the count rate at a satisfactory level. After three or four runs when the oven temperature approached 550 °C, the system was turned off and the soft-x-ray collection system recycled. It was feared from past experience that running the system at such elevated lithium fluxes would lead to its rapid destruction. The recycling at this point consisted simply of breaking vacuum and replacing the light pipe and washing the Be filter in an alcohol bath. Only modest pump-down

TABLE IV. Summary of results.

e-gun current (mA)	e-gun voltage (eV)	Low microwave power (W)	High microwave power (W)	Krypton pressure (Torr)	Number of runs	$\mathcal{S}$ (MHz)
9	650	1.5	6.0	2×10^{-6}	29	62 767.2± 32.9
6	650	1.5	6.0	2×10^{-6}	10	62 760.1± 55.0
12	650	1.5	6.0	2×10^{-6}	7[a]	62 732.3± 100.2
9	450	1.5	6.0	2×10^{-6}	10	62 715.5± 44.8
9	650	1.5	6.0	6×10^{-6}	10	62 817.3± 57.5
9	650	2.5	6.0	2×10^{-6}	10	62 785.3± 42.1
				Total all runs	76	62 765.2± 20.9

[a] Data acquisition terminated before a set of ten runs could be completed here.

TABLE V. Results for standard runs broken down as a function of oven temperature.

Temperature (° C)	Number of runs	δ (MHz)
475–495	10	62 764.8 ± 41.8
495–515	9	62 678.1 ± 64.5
515–550	10	62 849.7 ± 45.9

and bake-out times (~1–2 days) were required to get the system operational again. After a total of about 20 runs a major overhaul of the IR flange assembly was necessary.

IX. RESULTS

The results of all precision runs are presented in Table IV. The data are broken down into subgroups taken with the same experimental parameters. The unweighted average Lamb shift result for each subgroup is tabulated along with its standard error. The first group of 29 runs represents data like those of Table III taken at some arbitrarily defined "standard conditions"; i.e., the apparatus seemed to run comfortably under these conditions and no systematic perturbations were anticipated. The remaining subgroups then represent attempts to determine experimentally if the result could be affected significantly by varying a single experimental parameter. The parameters varied were gun current, gun voltage, krypton pressure, and microwave power. No statistically significant difference between the standard-run results and the results for any of the other subgroups is apparent in Table IV. An attempt to see if the result was dependent on oven temperature was made by further breaking down the standard runs into subgroups of different temperature (see Table V). It is apparent that differences at the $1-2\sigma$ levels have been detected. However, there does not appear to be any systematic trend with temperature, and we conclude that these differences, like those of Table IV, are due to statistical fluctuations.

Since on theoretical grounds it is believed that the result should be free of systematic error to the statistical precision achieved, and no such effects were obviously detected, we conclude that the final uncertainty is determined predominantly by statistics. The final result is an unweighted average of all 76 runs taken at various parameter settings. We find $\delta = 62\,765 \pm 21$ MHz, where the uncertainty represents the standard error.

X. COMPARISON WITH THEORY

Many workers have contributed to the calculation of the terms in Eq. (1). A convenient summary of this elaborate QED calculation has been given by Taylor, Parker, and Langenberg.[33] Evaluating their equation (138) after correcting the fourth-order term according to Applequist and Brodsky[34] gives $\delta = 62\,754$ MHz for the Lamb shift in $^6Li^{2+}$. Here the fundamental constants as given in Ref. 33 have been employed and a value of $R = 2.50$ F has been taken for the nuclear radius. Erickson has privately communicated the result of his most recent calculation. He finds $\delta = 62\,762 \pm 9$ MHz, with the difference presumably originating from the inclusion of higher-order terms in $Z\alpha$. The experimental result reported here, $\delta = 62\,765 \pm 21$ MHz, is in apparent agreement with both of these theoretical values. In a paper now in preparation Erickson discusses how this and other high-Z Lamb-shift measurements probe various aspects of the theory and lead to physical information about electron structure, etc.

ACKNOWLEDGMENTS

I am deeply indebted to P. E. Havey for his extensive assistance with many aspects of this experiment. I would also like to thank the many people who have made useful comments over the long course of this work.

[1]S. Triebwasser, E. S. Dayhoff, and W. E. Lamb, Jr., Phys. Rev. 89, 98 (1953); R. T. Robiscoe, Phys. Rev. 168, 4 (1968); B. L. Cosens, Phys. Rev. 173, 49 (1968); E. Lipworth and R. Novick, Phys. Rev. 108, 1434 (1957); M. A. Narashimham and R. L. Strombotne, Phys. Rev. A 4, 14 (1971).

[2]M. Leventhal and P. E. Havey, Phys. Rev. Lett. 32, 808 (1974).

[3]C. Y. Fan, M. Garcia-Munoz, and I. A. Sellin, Phys. Rev. 161, 6 (1967).

[4]D. D. Dietrich, P. Lebow, B. DaCosta, R. deZafra, and H. Metcalf, Bull. Am. Phys. Soc. 19, 572 (1974).

[5]M. Leventhal, Nucl. Instrum. Methods 110, 343 (1973).

[6]R. Marrus (private communication).

[7]G. W. Erickson and D. R. Yennie, Ann. Phys. (N.Y.) 35, 271 (1965).

[8]G. W. Erickson, Phys. Rev. Lett. 27, 780 (1971).

[9]R. Novick, E. Lipworth, and P. F. Yergin, Phys. Rev. 100, 1153 (1955).

[10]S. L. Kaufman, W. E. Lamb, Jr., K. R. Lea, and M. Leventhal, Phys. Rev. A 4, 2128 (1971).

[11]S. Klarsfield, Phys. Lett. 30A, 382 (1969).

[12]H. A. Bethe and E. E. Salpeter, in *Handbuch der Physik*, edited by S. Flügge (Springer, Berlin, 1957), Vol. XXXV, p. 334.

[13]W. E. Lamb, Jr., and R. C. Retherford, Phys. Rev.

79, 549 (1950).
[14]H. A. Bethe and E. E. Salpeter, *Quantum Mechanics of One and Two Electron Atoms* (Springer, Berlin, 1957).
[15]W. E. Lamb, Jr., Phys. Rev. 85, 259 (1952).
[16]G. W. Erickson (private communications).
[17]G. W. Erickson (private communication). This value was not used in curve fitting.
[18]S. J. Brodsky and G. W. Erickson, Phys. Rev. 148, 26 (1966). We have evaluated all terms except for the unknown nuclear structure correction.
[19]A. Rich, Phys. Rev. Lett. 20, 967 (1968).
[20]J. H. E. Mattauch, W. Thiele, and A. H. Wapstra, Nucl. Phys. 67, 1 (1965).
[21]I. Lindgren, Ark. Fys. 29, 553 (1965).
[22]J. W. DuMond, Ann. Phys. (N.Y.) 7, 365 (1959).
[23]*Handbook of Chemistry and Physics*, 47th ed. (Chemical Rubber Co., Cleveland, 1967), p. E-65.
[24]E. P. Savinov and A. P. Lukirskii, Opt. Spectrosc. 23, 163 (1967).
[25]J. A. R. Samson, *Techniques of Vacuum Ultraviolet Spectroscopy* (Wiley, New York, 1967), p. 90.
[26]W. E. Lamb, Jr., and M. Skinner, Phys. Rev. 78, 539 (1950).
[27]T. Y. Wu and F. C. Yu, Chinese J. Phys. 5, 162 (1944).
[28]T. A. Carlson, C. C. Lu, T. C. Tucker, C. W. Nestor, and F. B. Malik, Oak Ridge National Laboratory Publ. No. ORNL-4614 (1970).
[29]T. Lucatorto, Ph.D. thesis (Columbia University, 1968) (unpublished).
[30]J. A. Giordmaine and T. C. Wang, J. Appl, Phys. 31, 463 (1960).
[31]R. H. McFarland and J. D. Kinney, Phys. Rev. 137, A1058 (1965).
[32]H. W. Kugel, M. Leventhal, and D. E. Murnick, Phys. Rev. A 6, 1306 (1972).
[33]B. N. Taylor, W. H. Parker, and D. N. Langenberg, Rev. Mod. Phys. 41, 375 (1969).
[34]T. Appelquist and S. J. Brodsky, Phys. Rev. Lett. 24, 562 (1970).
[35]M. Leventhal, D. E. Murnick, and H. W. Kugel, Phys. Rev. Lett. 28, 1609 (1972).
[36]G. P. Lawrence, C. Y. Fan, and S. Bashkin, Phys. Rev. Lett. 28, 1613 (1972).